HHS Public Access

Author manuscript

ACS Sustain Chem Eng. Author manuscript; available in PMC 2019 September 04.

Published in final edited form as:

ACS Sustain Chem Eng. 2018 September 4; 6(9): 11704–11715. doi:10.1021/acssuschemeng.8b01959.

Understanding Effects of PAMAM Dendrimer Size and Surface Chemistry on Serum Protein Binding with Discrete Molecular Dynamics Simulations

Bo Wang[#1,2], **Yunxiang Sun**[#1], **Thomas P. Davis**[3], **Pu Chun Ke**[3], **Yinghao Wu**[2], and **Feng Ding**[1,*]

[1]department of Physics and Astronomy, Clemson University, Clemson, SC 29634, USA

[2]Department of Systems and Computational Biology, Albert Einstein College of Medicine, Bronx, NY 10461, USA

[3]ARC Centre of Excellence in Convergent Bio-Nano Science and Technology, Monash Institute of Pharmaceutical Sciences, Monash University, 381 Royal Parade, Parkville, VIC 3052, Australia

[#] These authors contributed equally to this work.

Abstract

Polyamidoamine (PAMAM) dendrimers, a class of polymeric nanoparticles (NPs) with highly-controllable sizes and surface chemistry, are promising candidates for many biomedical applications, including drug and gene delivery, imaging, and inhibition of amyloid aggregation. In circulation, binding of serum proteins with dendritic NPs renders the formation of protein corona and alters the biological identity of the NP core, which may subsequently elicit immunoresponse and cytotoxicity. Understanding the effects of PAMAM size and surface chemistry on serum protein binding is, therefore, crucial to enable their broad biomedical applications. Here, by applying atomistic discrete molecular dynamics (DMD) simulations, we first uncovered the binding of PAMAM with HSA and Ig and detailed the dependences of such binding on PAMAM size and surface modification. Compared to either anionic or cationic surfaces, modifications with neutral phosphorylcholine (PC), polyethylene glycol (PEG), and hydroxyls (OH) significantly reduced binding with proteins. The relatively strong binding between proteins and PAMAM dendrimers with charged surface groups was mainly driven by electrostatic interactions as well as hydrophobic interactions. Using steered DMD (SDMD) simulations, we conducted a force-pulling experiment *in silico* estimating the critical forces separating PAMAM-protein complexes and deriving the corresponding free energy barriers for dissociation. The SDMD-derived HSA-binding affinities were consistent with existing experimental measurements. Our results highlighted the association dynamics of protein-dendrimer interactions and binding affinities, whose implications range from fundamental nanobio interfacial phenomena to the development of “stealth NPs”.

[*]**Corresponding Author** Feng Ding: fding@clemson.edu.

ASSOCIATED CONTENT

Supporting Information

The following files are available free of charge on line: Supplementary Figures S1-S4 in PDF format.

Conflicts of interest

The authors declare no conflicting interests.

TOC Figure:

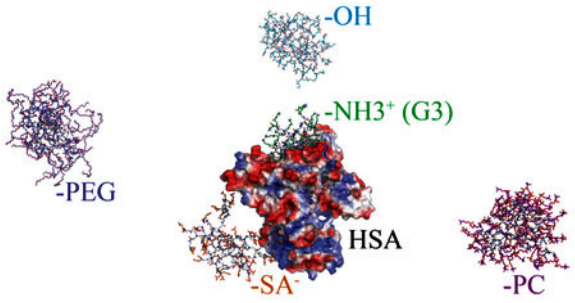

Understanding effects of dendritic polymer size and surface chemistry on the association with serum proteins ensures their sustainable biomedical applications

Keywords

PAMAM dendrimer; surface chemistry; serum protein binding; discrete molecular dynamics simulations; steered molecular dynamic simulations

Introduction

Dendrimers are a class of polymeric nanoparticles (NPs) with fractal-like structures, which can be precisely synthesized to assume high orders and mono-dispersity. The number of branching iterations emanating from the central core, named the “generation” of a dendrimer, defines its size.[1] The central core, branching units and terminal groups of a dendrimer can be individually selected, allowing for great design flexibility. PAMAM (polyamidoamine) dendrimers, featuring a diamine core and tertiary amine branching units, are one of the most commonly investigated dendrimers.[2,3] The structures and dynamics of PAMAM dendrimers have been well studied by both molecular dynamics (MD) simulations and experimental approaches such as small angle X-ray scattering (SAXS) and small angle neutron scattering (SANS).[4–8] PAMAM dendrimers typically adopt globular structures with the repeating units loosely packed in the interior and the surface groups solvated in solution. The dynamically forming pores in the interior can be used to encapsulate various guest molecules, including ions,[9,10] small molecules,[11–13] and peptides.[14–16] Surface groups of PAMAM can bind nucleotides for gene delivery[17] and also be readily modified by drugs or other functional ligands.[18,19] Because of their high versatility, PAMAM dendrimers have been explored for numerous applications, from environmental remediation[11,20] to drug and gene delivery, imaging, and inhibition of amyloid aggregation[2,15,17,21,22]

Upon entering circulation, NPs encounter proteins in the biological media to form a protein corona.[23–25] The protein corona shields the NP core and potentially compromises the designed functionalities.[26] The physicochemical properties of the NP-protein complex, rather than the pristine NP core, dictate their biological functions or pathological manifestations.[27,28] For example, the binding of NPs by opsonin proteins - e.g., immunoglobulin (Ig) and complement proteins in serum - may elicit immunoresponses,[29–33] which may subsequently promote the clearance of NPs, shorten their circulation lifetime,

and thus reduce the efficacy of nanomedicine. It is well established that the formation of a protein corona depends on the physicochemical properties of the NPs, such as their size, shape and surface chemistry.[34,35] Therefore, it is important to understand the binding of serum proteins and their dependence on NP size and surface chemistry in order to enable the applications of dendritic NPs.[36]

Experimental studies using amine-terminated PAMAM dendrimers without surface modifications have demonstrated the formation of serum protein coronae, including complement proteins[36], Ig proteins[37,38], and transport proteins like human serum albumin (HSA).[39] Recent studied from biomedicine revealed that IgE could recognize PAMAM-based antigens.[37] HSA is the most abundant serum protein, which can recognize and bind different biomolecules including ions, small molecule drugs, and peptides.[40–42] HSA binding has been shown to enhance the circulation of certain drugs.[43,44] Using HSA as a model serum protein, the dependence of protein binding affinities on PAMAM size and surface modifications was measured.[45] Amine-terminated PAMAM dendrimers could interact with membranes or membrane proteins to trigger structural disruption,[46,47] and also bind fibrinogens in serum to cause blood cloting.[48] Grafting dendrimers with neutral or anionic surface agents significantly eliminated nonspecific protein binding and reduced cytotoxic and hemolysis.[49–53] For instance, anionic PAMAM dendrimers have a confirmed high biocompatibility within the lung tissue.[52] Dendrimer-zwitterion conjugates displayed better protein resistance than their PEGylated counterpart for enhanced blood pool, lymph node and tumor CT imaging.[53] While many of these experimental studies provided insights to serum protein binding and corona formation, the molecular details of these inter-molecular interactions and the dependence on dendrimer size and surface chemistry remain poorly understood, as evidenced by the sometimes-inconsistent conclusions with respect to the binding and unfolding mechanisms (e.g., hydrophobic vs electrostatic, cationic surface vs anionic surface). Computational modeling therefore provides a useful approach to complement experimental studies and to derive a comprehensive picture of these biologically and biomedically important inter-molecular interactions.

Previous computational studies have been mainly focused on the structures and dynamics of dendrimers, dependence on dendrimer size and surface chemistry, as well as solvent conditions.[4,8,14,54–56] Small molecule binding has also been extensively studied.[12,20,57] While MD simulations of PAMAM alone offered structural insight to their binding with HAS,[45] the molecular details of protein-PAMAM binding[58,59] were unknown due to the large molecular systems whose time and length scales were inaccessible to traditional MD approaches. Recently, all-atom discrete molecular dynamics simulations (DMD, a rapid and predictive MD algorithm[60]) have been used to capture the structures and dynamics of PAMAM dendrimers of different sizes and surface modifications, showing agreement with previous experimental and computational studies,[13] including the binding of various proteins such as HSA[61] and NPs.[25,62] With multiple optimization implemented, including implicit solvent treatment and step-wise potential functions (details see Methods), DMD entailed a large sampling volume from both temporal and spatial spaces, thereby offering new opportunities to simulate large molecular systems and providing new molecular details that are often difficult to obtain from experimental techniques. In this study, specifically, we applied atomistic DMD simulations to systematically study the binding of HSA and IgE as

representative serum proteins to PAMAM dendrimers of different sizes (generations 1 to 4) and surface chemistry, including positively charged amine (NH_2), negatively charged succinamic acid (SA), and neutral hydroxyls (OH), polyethylene glycol (PEG)[63] and phosphorylcholine (PC). Surface modifications with PEG are the gold standard in the field of nanomedicine, in order to reduce nonspecific protein binding and increase blood circulation.[64–67] PC, the zwitterionic head group of phospholipids forming cell membranes, has been recently demonstrated as an excellent alternative to PEG for reduced protein binding.[61,68,69] We found that compared to either anionic or cationic surfaces, modifications with neutral PC, PEG, and OH significantly reduced protein fouling. The relatively strong binding between proteins and charged PAMAM dendrimers was mainly governed by electrostatic interactions since most proteins simultaneously contain both positively and negatively charged moieties on their surfaces. In addition, bound dendrimers may change their conformation for maximum binding, including facilitating hydrophobic interactions. For charged PAMAM dendrimers where the formation of dendrimer-protein complexes was observed in simulations, we applied steered DMD (SDMD) simulations to estimate the critical forces required to break inter-molecular interactions and also their corresponding free energy barriers of dissociation. This *in silico* experiment is of high relevance since force-pulling has recently been performed with atomic force microscopy for characterizing the interaction of PAMAM dendrimer and folate-binding protein.[70] The SDMD-derived HSA-binding affinities for PAMAM dendrimers of different sizes and surface chemistries were consistent with previous experimental measurements.[45] Our results highlighted the importance of surface modifications with zwitterionic ligands to reduce nonspecific protein binding for the design of stealthy NPs.

Computational Methods Section

Discrete molecular dynamics.

DMD is a special form of MD algorithm, where the conventional continuous potentials are replaced by step-wise functions.[71,72] A comprehensive description of the DMD algorithm has been published elsewhere.[60,73] Briefly, a united-atom model with implicit solvent is used to represent a molecular system, in which all heavy atoms and polar hydrogen atoms of proteins and PAMAM dendrimers are explicitly modeled. Interatomic interactions are adapted from the Medusa force field,[74,75] which include *van der Waals* (VDW), solvation, hydrogen bond, and electrostatic interactions. The force field parameters for VDW, covalent bonds, bond angles and dihedrals are taken from CHARMM19.[76] An implicit model proposed by Lazaridis and Karplus, the EEF1 for the CHARMM19 force field,[77] is used to estimate the solvation energy. The distance- and angular-dependent hydrogen bond interaction is modeled using a reaction-like algorithm.[78] Screened electrostatic interactions are computed by the Debye-Hückel approximation, where a Debye length of ~1 nm is used by assuming a water dielectric constant of 80 and a monovalent electrolyte concentration of 0.1 M. Counter ions (Cl^- or Na+) are added accordingly to maintain zero net charge of a simulated system and account for the counter-ion condensation effect in highly charge systems.[79] Periodic boundary condition is applied. All simulations are performed at 300K using the Anderson's thermostat.[80]

Dendrimers of different size and surface chemistry.

There same structural parameters as in our previous studies were used to model PAMAM dendrimers.[12,13,15] Specifically, we constructed the unmodified PAMAM dendrimers from generation 1 to 4 (G1-G4), whose terminal groups were amine (NH_2). At neutral pH, terminal primary amines were protonated with positive changes and interior secondary or tertiary amines were neutral. The negatively charged PAMAM corresponded to a generation of 3.5 (G3.5), where the terminal groups were succinamic acid (PAMAM-SA). The OH-terminated (PAMAM-OH) and PC-terminated (PAMAM-PC) dendrimers were constructed by modifying the terminal groups of a generation 4 PAMAM dendrimer (PAMAM-G4). The PEG-terminated PAMAM dendrimer (PAMAM-PEG) was constructed by conjugating the terminal groups of a generation 3 PAMAM dendrimer with PEG-10 ($-[O-CH_2-CH_2]_{10}-OH$), such that it had a comparable molecular weight to the other two neutrally charged dendrimers. Schematic chemical structures of all the terminal groups are illustrated in the inset of Fig. 1.

The Medusa force field has already been benchmarked not only for proteins[60,81] but also for small molecule ligands.[75,82] As a result, Medusa-based DMD simulations were able to accurately capture the structure and dynamics of PAMAM dendrimers[13], as well as their binding with different hydrocarbon molecules[12] and amyloid peptides.[15]

Modeling of proteins

The atomic coordinates from Protein Data Bank (PDB)[83] were used for both HSA (chain A; PDB ID: 1AO6) and IgE (chain A for the light chain and chain B for the heavy chain; PDB ID: 3HR5) (Fig. S1). For both proteins, basic and acidic amino acids were assigned charges according to their titration states at physiological condition (pH=7.4) - i.e., Arg and Lys were assigned +1e, Asp and Glu were assigned −1e, while His was neutral. Given the large protein sizes (e.g., ~440 and 580 amino acids in IgE and HSA, respectively), we only allowed dendrimers free to move, but kept HSA and IgE immobilized except all charged residues.

DMD simulations of protein-dendrimer binding.

We kept one protein and one dendrimer for the binding simulations. For each protein-dendrimer system, fourteen independent simulations were performed starting from randomly generated configurations with different intermolecular distances (larger 2nm) and orientations. Each independent simulation lasted 75 ns and an accumulative 1.05 p,s DMD simulations for each protein-dendrimer pair were executed. To avoid a potential bias from initial conformation, the first 25 ns trajectory of each independent simulation was discarded in the analysis of inter-molecular binding.

Steered discrete molecular dynamics.

Steered MD (SMD) is widely used for evaluating protein-ligand binding[84,85] and mechanically-induced unfolding of proteins.[86–88] As in force pulling experiments with AFM, either constant force or constant pulling velocity could be used in SMD. In our study, we adopted the constant force protocol to investigate the binding in our steered DMD (SDMD) simulations, where the constant pulling force was deployed between a pair of

atoms via a step-wise potential function with a potential energy jump of dE at every step of dR - *i.e.*, the force $F = dE/dR$. The force can be adjusted by tuning either dE or dR. For instance, the force corresponding to a potential energy change dE = 1 kcal/mole at a distance interval dR = 1 A is equivalent to ~70 *pN*.

For a given protein-dendrimer pair, the most stable molecular complex was subject to force pulling in SDMD. Specifically, we selected the bound state with lowest potential energy out of all independent binding simulations discussed above as the starting confirmation for SDMD simulations to estimate the corresponding inter-molecular binding affinities. A selected dendrimer-protein complex was then subject to a set of forces applied between their centers of mass as discussed above in DMD simulations. Given the high complexity of the free energy landscape, we performed for each force ten independent pulling simulations to ensure sufficient sampling, where the initial atomic velocities were randomized according to the Maxwell-Boltzmann distribution. The force range in each protein-dendrimer system was from zero to 175 pN. An interval of 8.75 pN was assigned to the range from zero to 87.5 pN, while a larger interval of 17.5 pN was assigned to the range of 87.5 pN to 175 pN. Each independent constant force SDMD simulations lasted 30 ns and the mean first massage time of dissociation was computed as bellow.

Derivation of critical forces for dissociation.

The dissociation time of a protein-dendrimer was governed by a free energy barrier, $\Delta G^{\neq}$, at the inter-molecular distance, $d^{\neq}$, mainly due to the loss of inter-molecular interactions - i.e., $\sim exp(\beta \Delta G^{\neq})$. Here, β equals to the inverse of $k_b T$, k_b is the Boltzmann constant and T is the temperature. Under a given force F, the barrier was reduced by $\sim F^* \Delta d$, where $\Delta d = d^{\neq} - d^{eq}$ and d^{eq} denoted the equilibrium inter-molecular distance. In our simulations, we estimated the dissociation time by computing the mean first passage time (MFPT) of dissociation, t_{MPFT}, from monitoring the number of inter-molecular contacts (Fig. S3A).

Under weak forces where the barrier still existed and assuming $d^{\neq}$ and d^{eq} remained the same under different forces, the logarithm of t_{MPFT} linearly decreased with respect to the force, $\sim (\Delta G^{\neq} - F^* \Delta d)$. The critical force F_c corresponded to the force that rendered the barrier zero. As the force increased beyond Fc and barrier no longer existed, the dissociation was analogous to diffusion under a net force, ~(F-F_c), with frictions. Under the weak force approximation in the barrier-less dissociation regime, the logarithm of t_{MPFT} also linearly decreased with respect to the net force.[89] Hence, we estimated the critical force by plotting the logarithm of $tMPFT$ as a function of force and linearly fitting the function in both barrier and barrier-less regions (Fig. S3B).[88] The intersection of the two linear fits determined F_c. We used error bars of the linear regression to estimate the error bards of F_c via the error propagation.

Results and Discussion

Dendrimers of different sizes and surface modifications.

To account for the size effect, we studied unmodified PAMAM dendrimers from generations 1 to 4 (G1-G4), where the number of positively charged terminal amine groups increased

from 8 (2^3) to 64 (2^6) correspondingly (Fig. 1). We included modified PAMAM dendrimers with negatively charged carboxyl (PAMAM-SA) and neutrally changed groups of hydroxyl (PAMAM-OH), polyethylene glycol (PAMAM-PEG), and phosphorylcholine (PAMAM-PC). All PAMAM derivatives were constructed with similar sizes to ensure a reasonable comparison for their binding with proteins (details see Methods). As observed previously,[13] PAMAM dendrimers equilibrated rapidly in DMD simulations (equilibrated snapshot structures in Fig. 1). The computed equilibrium radii of gyration (Rg) of different PAMAM dendrimers were consistent with previous experiments and computational simulations (Fig. 1A).[4–8] For unmodified PAMAM dendrimers, the size increased monotonically with the increasing number of generations. PAMAM-SA corresponded to a generation of 3.5 and thus had *Rg* values between PAMAM-G3 and PAMAM-G4. With the same generation as PAMAM-G4, PAMAM-OH significantly collapsed due to the formation of extensive hydrogen bonds among terminal hydroxyls and also between hydroxyls and interior amidoamine groups. PAMAM-PEG and PAMAM-PC were constructed from PAMAM-G3, featuring intermediate Rg values between PAMMA-G3 and PAMAM-G4. Different from PAMAM-OH, the PC and PEG terminal groups tended to be solvated due to their high water solubility[61] (Fig. 1).

The dependence of serum protein binding on PAMAM dendrimer size and surface chemistry.

We used HSA and IgE as model serum proteins to study their binding with PAMAM dendrimers (Methods). IgE and HSA are generally stable and comprise 440 and 580 residues each. Given the large protein sizes, we allowed the dendrimers free to move, but kept HSA and IgE immobilized except all charged residues, which were able to sample their side-chain conformations to achieve optimal binding with charged dendrimers. In drug/gene delivery applications, the dendrimer concentration is much lower than that of HSA and Ig proteins during circulation, leading to a substoichiometry in binding. Given PAMAM dendrimers are soft polymeric NPs[90] that can change their conformation upon binding with proteins, and also considering the low nanoparticle concentration in serum, minimal backbone perturbations to both HSA and IgE were plausible. Despite these simplifications to reduce simulation cost, we noted that there were 179 charged amino acids in HSA and 73 in IgE.

To derive fundamental association dynamics of the systems and screen the potential binding sites on proteins, our DMD simulations followed the common usage of 1:1 molecular ratio, i.e., one protein and one PAMAM dendrimer with periodic boundary conditions. For each protein-dendrimer pair, multiple independent simulations starting from randomly generated conformation with different intermolecular distances (larger than 2 nm) and orientations were performed to ensure sufficient sampling (Methods). However, in experiments with controlled biomolecule concentrations, excessive dendrimers compared to proteins may form complex supramolecular complexes beyond the 1:1 stoichiometry,[91] as we previously observed with dendrimer-hydrocarbon binding.[12] Examination of simulation trajectories indicated that the neutrally charged PAMAM dendrimers bound proteins dynamically, and the charged dendrimers tended to stay bound to proteins for a longer time period while diffusions on the protein surface and dissociations from proteins were frequently observed. To quantify the binding of PAMAM dendrimers to proteins, we calculated the binding

frequencies of each protein residue with the dendrimer by averaging over all independent simulations for each dendrimer-protein pair (Fig. 2). A cutoff distance of 0.65 nm was used to define a contact between two heavy atoms, and two molecules interacted with each other by forming at least one intermolecular atomic contact. Indeed, HSA with a net charge of −15e had highly preferred binding sites for positively charged PAMAM-G1 to G4, displaying binding frequencies as high as ~80% (Fig. 2A). As expected, PAMAM-SA had less frequent binding to HSA residues compared to these unmodified dendrimers, but significantly more than the neutrally charged dendrimers. Both positively and negatively charged PAMAM dendrimers had binding sites on IgE (a net charge of +3e) with comparable frequencies (~10%), which were also significantly higher than those with neutrally charged dendrimers (Fig. 2B). As evident from the residue-wise binding frequency profiles, the same charged PAMAM-G1 to G4 with different sizes tended to have similar binding sites on proteins, while dendrimers with opposite or neutral charges usually bound to proteins differently.

Electrostatic interactions in the binding of charged dendrimers with proteins.

To visualize the dendrimer binding sites on proteins, we colored each residue according to its binding frequencies with dendrimers (Figs. 3&5). HSA residues with high binding frequencies to both positively (PAMAM-G1 to G4) and negatively charged (PAMAM-SA) dendrimers were all clustered together on the protein surface (Fig. 3A). The binding site to PAMAM dendrimers G1-G4 on the HSA surface corresponded to a large area with many acidic residues (e.g., E6, D13, E57, D63, E95, E218, E227, E230, D237, E244, E252, D256, E321) and thus negative electrostatic potentials. PAMAM-SA, on the other hand, bound to a smaller surface area containing multiple basic residues (e.g., K413, K414, K475, K536, K538, K541) with positive electrostatic potentials. Dendrimer-protein interactions have been described by different models. Shcharbin et al. proposed that PAMAM possessed 5–6 non-specific ‘binding sites’ on albumin based on local concentrations of charged amino acid residues on the protein surface.[58] Chiba et al. presented a ‘hot spot’ model illustrating dendrimer bound to the surface charged hotspot region of chymotrypsin and cytochrome-c.[92] Our current simulation (Fig. 3A) is in agreement with the above models. Moreover, dendrimers could undergo major conformational changes, not just for maximizing electrostatic interactions but also for hydrophobic interactions with the protein (Fig. 4A). The hydrophobic interior of PAMAM-G3 exposed to HSA surface, thereby contributing a complementary hydrophobic interaction. The significance of hydrophobic interaction in protein-dendrimer binding has been highlighted by a number of other studies.[93,94] For instance, Giri et al. suggested that the inner shell protons of PAMAM interacted more strongly with HSA.[45] Our current finding may help resolve the inconsistencies of dominated forces in dendrimer-protein interactions (electrostatic vs hydrophobic) concluded by different experiments.[45,93,36] A two-step process was plausibly involved in the interaction: PAMAM dendrimers first anchored on the HSA surface via electrostatic interaction, and hydrophobic interactions were consequently evoked via conformation changes. Similar phenomena have been observed in PAMAM-Ig interactions. PAMAM dendrimers G1 to G4 also had one preferred site on IgE surface with negative electrostatic potentials. Interestingly, the binding sites for these positively charged dendrimers corresponded to the well-known complementarity-determining regions (CDR) - CDR1, CDR2, and CDR3 loops (Fig. 3B and

Fig. 4B),[95] which are responsible for binding to specific antigens and are closely related to binding with major histocompatibility complex (MHC).[96] As positively charged PAMAM dendrimers are cytotoxic,[48] IgE could recognize the PAMAM via these loops, as evidenced by a recent experiment that multiepitope dendrimeric antigens (constructed based on PAMAM-G4) can be recognized by human IgE.[37] Considering neutrally charged dendrimer also bound CDR loops (details in the following section), our simulations provided important information concerning IgE-antigen recognition. PAMAM-SA had more than one binding site on IgE, all of which corresponded to patches with positive electrostatic potentials and one of which was preferred with a higher dendrimer binding frequency (Fig. 3B).

Weak and dynamic protein binding by neutrally charged PAMAM dendrimers.

Neutrally charged dendrimers usually possessed multiple binding sites on both HSA and IgE (Fig. 5A). PAMAM-PC had similar binding sites on HSA as PAMAM-OH (also see Fig. 2A), although each binding site for PAMAM-PC had larger surface areas. This observation suggests that PAMAM-PC and PAMAM-OH shared similar binding interactions with HSA, and the difference was likely due to the more packed 3D structure of PAMAM-OH than that of PAMAM-PC (Fig. 1B and Fig. S2A). PAMAM-PEG, on the other hand, had completely different binding to HSA than PAMAM-OH and PAMAM-PC, likely due to the outer PEG moieties (Figure. S2B). Compared to HSA, IgE tended to have more residues involved in binding with these neutrally charged dendrimers and more similar binding profiles to the three different dendrimers (Fig. 5B and Fig. 2B). Specifically, the CDR loops had a tendency to bind all three types of neutrally charged dendrimers, underscoring the unique function of these loops in recognizing antigens.

To further compare the binding of neutrally charged PAMAM dendrimers with proteins, we computed for each dendrimer-protein pair the histogram of binding frequencies per residue to the dendrimer (Fig. 5C). Compared to HSA, the slower decrease in the log-log plot for IgE was consistent with the observation that IgE had more residues involved in the binding with these neutrally charged dendrimers and also the functional role of IgE in recognition versus HSA in transportation. Interestingly, OH and PC displayed faster decreases in the log-log plot than PEG, suggesting that OH and PC terminated dendrimers tended to have weaker binding frequencies to proteins. Hence, these results suggest that OH and PC might serve as alternative antifouling agents against nonspecific or specific protein binding.

Free energy barrier of dissociation estimation using steered DMD simulations.

Steered MD simulations utilize a similar approach as single-molecule force spectroscopy techniques to evaluate protein-ligand binding affinity *in silico*.[87,97,98] Typically, the probed protein-ligand complexes feature a two-state dynamics between bounded and unbound states. Here, we applied SDMD simulations (details see Methods) to estimate the binding between proteins and the charged dendrimers, which revealed the formation of stable protein-dendrimer complexes in binding simulations above. Briefly, we applied constant forces separating protein and dendrimer from their bounded state, and performed multiple independent simulations with randomized velocities to estimate the mean first passage time of dissociation (MFPT) as the approximation for dissociation time (Fig. 6). The dissociation

time decreased with increasing forces and different protein-dendrimer complexes required different forces to dissociate from each other.

The applied force, F, decreased the free energy barrier for dissociation, and the critical force, Fc, rendered the dissociation barrier zero. Hence, the dissociation dynamics underwent a transition from a barrier-ed (i.e., activation-dependent) to a barrier-less (i.e., diffusion under a net force of $F\text{-}Fc$ with frictions) process, featuring different dependence characteristics on the applied force (see Methods). We quantified the critical force by determining the crossover point (Fig. 7A&B). As expected, the low generation dendrimers were more sensitive to the growing forces and were more readily dissociated from protein while high generation dendrimers were more robustly bound to proteins requiring a high level of critical forces.

The free energy barrier for dissociation $\Delta G^{\neq}$ equaled to the work done by the critical force Fc to dissociate the complex, which required the estimation of distance between equilibrium and force-induced dissociation, i.e., the effective pulling distance Δd. By analyzing the histogram of intermolecular distances, $d_{NP\text{-}protein}$, and also the dependence of the number of intermolecular contacts as the function of $d_{NP\text{-}protein}$ (Fig. S4), we were able to determine Δd and thus $\Delta G^{\neq}=Fc*\Delta d$ (Fig. 7C&D). The binding affinity ΔG is related to the binding constant K_b, $\Delta G = - RTlnK_b$. As the binding constant is defined by both association rate k_{on} and dissociation rate k_{off}, the binding affinity can be expressed as $-(RTlnk_{on} - RTlnk_{off})$. The SDMD performed in our study only considered the contribution from dissociation, i.e., $\Delta G^{\neq} \sim RTlnk_{off}$. Association rate (commonly approximated by the diffusion limit) could be affected by many factors, such as buffer, ionic strength and pH, leading to different values in experimental measurements (Table 1). However, similar trends were expected in terms of protein binding with dendrimers of different generations or surface chemistry. Indeed, the dissociation free energy barriers $\Delta G^{\neq}$ agreed well with previous experimental measurement of binding affinities between HSA and dendrimers of different sizes and surface chemistry,[45] where the binding affinities increased with increasing sizes. Although the binding of negatively charged PAMAM-SA required a relative weak force to separate its binding from the overall negatively charged protein (e.g., with a value between those of G1 and G2), the high conformational flexibility upon dissociation resulted in a dissociation free energy barrier $\Delta G^{\neq}$ comparable to that of PAMAM-G4, suggesting a surprisingly strong HSA-binding affinity, in agreement with experimental measurements.[45]

Conclusion

In summary, we applied atomistic DMD simulations to systematically investigate the molecular details of the binding between primary serum proteins, HSA and IgE, with PAMAM dendrimers of different sizes and surface modifications. Despite the difference between HSA and IgE in terms of size, secondary structure, and net charge, both proteins displayed relatively strong binding with either positively or negatively charged PAMAM dendrimers. The strong binding was governed by electrostatic interactions since all proteins possess both positively and negatively charged moieties, forming mosaic like surface patches with either negative or positive electrostatic potentials (Fig. 3). Neutrally charged PAMAM dendrimers, on the other hand, showed dynamic and weak binding to both proteins. Binding

analysis indicated that, comparing to HSA, IgE whose function was to bind antigens tended to administer more contacts with neutrally charged dendrimers, especially by its CDR loops. Since the binding of proteins, especially by opsonin proteins like IgE, may elicit immunoresponse and reduce the circulation lifetime of NPs, our results suggest that surface modifications by neutrally charged, polar agents instead of charged groups can efficiently reduce specific or nonspecific protein binding, i.e., achieving the anti-fouling effect. Our results also suggest that both hydroxyl and phosphorylcholine are excellent alternative to PEG as anti-fouling agents against serum proteins, at least for the most abundant species of HSA and IgE. We also applied steered DMD simulations to study the binding affinity between the serum proteins and charged PAMAM dendrimers. Using stable complexes derived from binding simulations, dendrimers were pulled away from the proteins by a set of constant forces, where the dissociation times were determined as a function of applied forces. By estimating both the critical forces and the work done to separate the dendrimer-protein complexes, the free energy barriers for dissociation (or the off-rates) were also calculated. The computational results were consistent with experimentally measured binding affinities of HSA with PAMAM dendrimers of different sizes and surface chemistry, vindicating the predictive power of the DMD methodology. Together, our study offered a mechanistic insight to the binding of serum proteins with NPs of different sizes and surface modifications, and should prove valuable for the design of biocompatible and stealthy nanomedicines.

Supplementary Material

Refer to Web version on PubMed Central for supplementary material.

ACKNOWLEDGMENT

This work was supported in part by NSF CBET-1553945 (Ding), NIH R35GM119691 (Ding), and ARC Project No. CE140100036 (Davis).

REFERENCES

(1). Helms B; Meijer EW Dendrimers at Work. Science 2006, 313 (5789), 929–930, DOI 10.1126/science.1130639. [PubMed: 16917051]

(2). Svenson S; Tomalia DA Dendrimers in Biomedical Applications--Reflections on the Field. Adv. Drug Deliv. Rev 2005, 57 (15), 2106–2129, DOI 10.1016/j.addr.2005.09.018. [PubMed: 16305813]

(3). Tian W; Ma Y Theoretical and Computational Studies of Dendrimers as Delivery Vectors. Chem. Soc. Rev 2012, 42 (2), 705–727, DOI 10.1039/C2CS35306G.

(4). Maiti PK; Qağin T; Wang G; Goddard WA Structure of PAMAM Dendrimers: Generations 1 through 11. Macromolecules 2004, 37 (16), 6236–6254, DOI 10.1021/ma035629b.

(5). Chen W-R; Porcar L; Liu Y; Butler PD; Magid LJ Small Angle Neutron Scattering Studies of the Counterion Effects on the Molecular Conformation and Structure of Charged G4 PAMAM Dendrimers in Aqueous Solutions. Macromolecules 2007, 40 (16), 5887–5898, DOI 10.1021/ma0626564.

(6). Prosa TJ; Bauer BJ; Amis EJ From Stars to Spheres: A SAXS Analysis of Dilute Dendrimer Solutions. Macromolecules 2001, 34 (14), 4897–4906, DOI 10.1021/ma0002186.

(7). Liu Y; Chen C-Y; Chen H-L; Hong K; Shew C-Y; Li X; Liu L; Melnichenko YB; Smith GS; Herwig KW; et al. Electrostatic Swelling and Conformational Variation Observed in High-

Generation Polyelectrolyte Dendrimers. J. Phys. Chem. Lett 2010, 1 (13), 2020–2024, DOI 10.1021/jz1006143.

(8). Yang L; da Rocha SRP PEGylated, NH2-Terminated PAMAM Dendrimers: A Microscopic View from Atomistic Computer Simulations. Mol. Pharm 2014, 11 (5), 1459–1470, DOI 10.1021/mp400630z. [PubMed: 24679335]

(9). Diallo MS; Balogh L; Shafagati A; Johnson JH; Goddard WA, iii; Tomalia DA Poly (Amidoamine) Dendrimers : A New Class of High Capacity Chelating Agents for Cu (II) Ions. Environ. Sci. Technol 1999, 33 (5), 820–824.

(10). Xu Y; Zhao D Removal of Copper from Contaminated Soil by Use of Poly(Amidoamine) Dendrimers. Environ. Sci. Technol 2005, 39 (7), 2369–2375. [PubMed: 15871278]

(11). Bhattacharya P; Conroy N; Rao AM; Powell B. a.; Ladner D. a.; Ke PC PAMAM Dendrimer for Mitigating Humic Foulant. RSC Adv 2012, 2 (21), 7997, DOI 10.1039/c2ra21245e.

(12). Wang B; Geitner NK; Davis TP; Ke PC; Ladner DA; Ding F Deviation from the Unimolecular Micelle Paradigm of PAMAM Dendrimers Induced by Strong Interligand Interactions. J. Phys. Chem. C 2015, DOI 10.1021/acs.jpcc.5b04991.

(13). Geitner NK; Wang B; Andorfer RE; Ladner DA; Ke PC; Ding F Structure-Function Relationship of PAMAM Dendrimers as Robust Oil Dispersants. Environ. Sci. Technol 2014, 48 (21), 12868–12875, DOI 10.1021/es5038194. [PubMed: 25279688]

(14). Maiti PK; Li Y; Cagin T; Goddard WA Structure of Polyamidoamide Dendrimers up to Limiting Generations: A Mesoscale Description. J. Chem. Phys 2009, 130 (14), 144902, DOI 10.1063/1.3105338. [PubMed: 19368466]

(15). Gurzov EN; Wang B; Pilkington EH; Chen P; Kakinen A; Stanley WJ; Litwak SA; Hanssen EG; Davis TP; Ding F; et al. Inhibition of HIAPP Amyloid Aggregation and Pancreatic β-Cell Toxicity by OH-Terminated PAMAM Dendrimer. Small Weinh. Bergstr. Ger 2016, 12 (12), 1615–1626, DOI 10.1002/smll.201502317.

(16). Lin S-T; Maiti PK; Goddard WA Dynamics and Thermodynamics of Water in PAMAM Dendrimers at Subnanosecond Time Scales. J. Phys. Chem. B 2005, 109 (18), 8663–8672, DOI 10.1021/jp0471958. [PubMed: 16852026]

(17). Esfand R; Tomalia DA Poly(Amidoamine) (PAMAM) Dendrimers: From Biomimicry to Drug Delivery and Biomedical Applications. Drug Discov. Today 2001, 6 (8), 427–436, DOI 10.1016/S1359-6446(01)01757-3. [PubMed: 11301287]

(18). Luo D; Haverstick K; Belcheva N; Han E; Saltzman WM Poly(Ethylene Glycol-Conjugated PAMAM Dendrimer for Biocompatible, High-Efficiency DNA Delivery. Macromolecules 2002, 35 (9), 3456–3462, DOI 10.1021/ma0106346.

(19). Chandrasekar D; Sistla R; Ahmad FJ; Khar RK; Diwan PV The Development of Folate-PAMAM Dendrimer Conjugates for Targeted Delivery of Anti-Arthritic Drugs and Their Pharmacokinetics and Biodistribution in Arthritic Rats. Biomaterials 2007, 28 (3), 504–512, DOI 10.1016/j.biomaterials.2006.07.046. [PubMed: 16996126]

(20). DeFever RS; Geitner NK; Bhattacharya P; Ding F; Ke PC; Sarupria S PAMAM Dendrimers and Graphene: Materials for Removing Aromatic Contaminants from Water. Environ. Sci. Technol 2015, 49 (7), 4490–4497, DOI 10.1021/es505518r. [PubMed: 25786141]

(21). Barrett T; Ravizzini G; Choyke PL; Kobayashi H Dendrimers Application Related to Bioimaging. IEEE Eng. Med. Biol. Mag. Q. Mag. Eng. Med. Biol. Soc 2009, 28 (1), 12–22, DOI 10.1109/MEMB.2008.931012.

(22). Lee CC; MacKay JA; Frechet JMJ; Szoka FC Designing Dendrimers for Biological Applications. Nat. Biotechnol 2005, 23 (12), 1517–1526, DOI 10.1038/nbt1171. [PubMed: 16333296]

(23). Casals E; Pfaller T; Duschl A; Oostingh GJ; Puntes V Time Evolution of the Nanoparticle Protein Corona. ACS Nano 2010, 4 (7), 3623–3632, DOI 10.1021/nn901372t. [PubMed: 20553005]

(24). Cedervall T; Lynch I; Lindman S; Berggard T; Thulin E; Nilsson H; Dawson KA; Linse S Understanding the Nanoparticle-Protein Corona Using Methods to Quantify Exchange Rates and Affinities of Proteins for Nanoparticles. Proc. Natl. Acad. Sci 2007, 104 (7), 2050–2055, DOI 10.1073/pnas.0608582104. [PubMed: 17267609]

(25). Ding F; Radic S; Chen R; Chen P; Geitner NK; Brown JM; Ke PC Direct Observation of a Single Nanoparticle-Ubiquitin Corona Formation. Nanoscale 2013, 5 (19), 9162–9169, DOI 10.1039/c3nr02147e. [PubMed: 23921560]

(26). Salvati A; Pitek AS; Monopoli MP; Prapainop K; Bombelli FB; Hristov DR; Kelly PM; Åberg C; Mahon E; Dawson KA Transferrin-Functionalized Nanoparticles Lose Their Targeting Capabilities When a Biomolecule Corona Adsorbs on the Surface. Nat. Nanotechnol 2013, 8 (2), 137–143, DOI 10.1038/nnano.2012.237. [PubMed: 23334168]

(27). Lundqvist M; Stigler J; Elia G; Lynch I; Cedervall T; Dawson KA Nanoparticle Size and Surface Properties Determine the Protein Corona with Possible Implications for Biological Impacts. Proc. Natl. Acad. Sci 2008, 105 (38), 14265–14270, DOI 10.1073/pnas.0805135105. [PubMed: 18809927]

(28). Hellstrand E; Lynch I; Andersson A; Drakenberg T; Dahlback B; Dawson KA; Linse S; Cedervall T Complete High-Density Lipoproteins in Nanoparticle Corona. FEBS J 2009, 276 (12), 3372–3381, DOI 10.1111/j.1742-4658.2009.07062.x. [PubMed: 19438706]

(29). Maas C; Hermeling S; Bouma B; Jiskoot W; Gebbink MFBG A Role for Protein Misfolding in Immunogenicity of Biopharmaceuticals. J. Biol. Chem 2007, 282 (4), 2229–2236, DOI 10.1074/jbc.M605984200. [PubMed: 17135263]

(30). Deng ZJ; Liang M; Monteiro M; Toth I; Minchin RF Nanoparticle-Induced Unfolding of Fibrinogen Promotes Mac-1 Receptor Activation and Inflammation. Nat. Nanotechnol 2011, 6 (1), 39–44, DOI 10.1038/nnano.2010.250. [PubMed: 21170037]

(31). Elsabahy M; Wooley KL Cytokines as Biomarkers of Nanoparticle Immunotoxicity. Chem. Soc. Rev 2013, 42 (12), 5552–5576, DOI 10.1039/c3cs60064e. [PubMed: 23549679]

(32). Lesniak A; Fenaroli F; Monopoli MP; Aberg C; Dawson KA; Salvati A Effects of the Presence or Absence of a Protein Corona on Silica Nanoparticle Uptake and Impact on Cells. ACS Nano 2012, 6 (7), 5845–5857, DOI 10.1021/nn300223w. [PubMed: 22721453]

(33). Hu W; Peng C; Lv M; Li X; Zhang Y; Chen N; Fan C; Huang Q Protein Corona-Mediated Mitigation of Cytotoxicity of Graphene Oxide. ACS Nano 2011, 5 (5), 3693–3700, DOI 10.1021/nn200021j. [PubMed: 21500856]

(34). Albanese A; Tang PS; Chan WCW The Effect of Nanoparticle Size, Shape, and Surface Chemistry on Biological Systems. Annu. Rev. Biomed. Eng 2012, 14 (1), 1–16, DOI 10.1146/annurev-bioeng-071811-150124. [PubMed: 22524388]

(35). Monopoli MP; Walczyk D; Campbell A; Elia G; Lynch I; Bombelli FB; Dawson KA Physical-Chemical Aspects of Protein Corona: Relevance to in Vitro and in Vivo Biological Impacts of Nanoparticles. J. Am. Chem. Soc 2011, 133 (8), 2525–2534, DOI 10.1021/ja107583h. [PubMed: 21288025]

(36). Shcharbin D; Shcharbina N; Dzmitruk V; Pedziwiatr-Werbicka E; Ionov M; Mignani S; de la Mata FJ; Gomez R; Munoz-Fernandez MA; Majoral J-P; et al. Dendrimer-Protein Interactions versus Dendrimer-Based Nanomedicine. Colloids Surf. B Biointerfaces 2017, 152, 414–422, DOI 10.1016/j.colsurfb.2017.01.041. [PubMed: 28167455]

(37). Montañez MI; Najera F; Mayorga C; Ruiz-Sanchez AJ; Vida Y; Collado D; Blanca M; Torres MJ; Perez-Inestrosa E Recognition of Multiepitope Dendrimeric Antigens by Human Immunoglobulin E. Nanomedicine Nanotechnol. Biol. Med 2015, 11 (3), 579–588, DOI 10.1016/j.nano.2015.01.006.

(38). Lin J; Hua W; Zhang Y; Li C; Xue W; Yin J; Liu Z; Qiu X Effect of Poly(Amidoamine) Dendrimers on the Structure and Activity of Immune Molecules. Biochim. Biophys. Acta BBA - Gen. Subj 2015, 1850 (2), 419–425, DOI 10.1016/j.bbagen.2014.11.016.

(39). Akesson A; Cardenas M; Elia G; P. Monopoli M; A. Dawson K The Protein Corona of Dendrimers: PAMAM Binds and Activates Complement Proteins in Human Plasma in a Generation Dependent Manner. RSC Adv 2012, 2 (30), 11245–11248, DOI 10.1039/C2RA21866F.

(40). Bal W; Sokotowska M; Kurowska E; Faller P Binding of Transition Metal Ions to Albumin: Sites, Affinities and Rates. Biochim. Biophys. Acta BBA - Gen. Subj 2013, 1830 (12), 5444–5455, DOI 10.1016/j.bbagen.2013.06.018.

(41). Tabassum S; Al-Asbahy WM; Afzal M; Arjmand F Synthesis, Characterization and Interaction Studies of Copper Based Drug with Human Serum Albumin (HSA): Spectroscopic and Molecular Docking Investigations. J. Photochem. Photobiol. B 2012, 114, 132–139, DOI 10.1016/j.jphotobiol.2012.05.021. [PubMed: 22750083]

(42). Kuo Y-M; Kokjohn TA; Kalback W; Luehrs D; Galasko DR; Chevallier N; Koo EH; Emmerling MR; Roher AE Amyloid-β Peptides Interact with Plasma Proteins and Erythrocytes: Implications for Their Quantitation in Plasma. Biochem. Biophys. Res. Commun 2000, 268 (3), 750–756, DOI 10.1006/bbrc.2000.2222. [PubMed: 10679277]

(43). Yang F; Zhang Y; Liang H Interactive Association of Drugs Binding to Human Serum Albumin. Int. J. Mol. Sci 2014, 15 (3), 3580–3595, DOI 10.3390/ijms15033580. [PubMed: 24583848]

(44). Mandula H; Parepally JMR; Feng R; Smith QR Role of Site-Specific Binding to Plasma Albumin in Drug Availability to Brain. J. Pharmacol. Exp. Ther 2006, 317 (2), 667–675, DOI 10.1124/jpet.105.097402. [PubMed: 16410405]

(45). Giri J; Diallo MS; Simpson AJ; Liu Y; Goddard WA; Kumar R; Woods GC Interactions of Poly(Amidoamine) Dendrimers with Human Serum Albumin: Binding Constants and Mechanisms. ACS Nano 2011, 5 (5), 3456–3468, DOI 10.1021/nn1021007. [PubMed: 21438566]

(46). Hong S; Bielinska AU; Mecke A; Keszler B; Beals JL; Shi X; Balogh L; Orr BG; Baker JR; Banaszak Holl MM Interaction of Poly(Amidoamine) Dendrimers with Supported Lipid Bilayers and Cells: Hole Formation and the Relation to Transport. Bioconjug. Chem 2004, 15 (4), 774–782, DOI 10.1021/bc049962b. [PubMed: 15264864]

(47). Kelly CV; Liroff MG; Triplett LD; Leroueil PR; Mullen DG; Wallace JM; Meshinchi S; Baker JR; Orr BG; Banaszak Holl MM Stoichiometry and Structure of Poly(Amidoamine) Dendrimer-Lipid Complexes. ACS Nano 2009, 3 (7), 1886–1896, DOI 10.1021/nn900173e. [PubMed: 19534489]

(48). Jones CF; Campbell RA; Brooks AE; Assemi S; Tadjiki S; Thiagarajan G; Mulcock C; Weyrich AS; Brooks BD; Ghandehari H; et al. Cationic PAMAM Dendrimers Aggressively Initiate Blood Clot Formation. ACS Nano 2012, 6 (11), 9900–9910, DOI 10.1021/nn303472r. [PubMed: 23062017]

(49). Malik N; Wiwattanapatapee R; Klopsch R; Lorenz K; Frey H; Weener JW; Meijer EW; Paulus W; Duncan R Dendrimers:: Relationship between Structure and Biocompatibility in Vitro, and Preliminary Studies on the Biodistribution of 125I-Labelled Polyamidoamine Dendrimers in Vivo. J. Controlled Release 2000, 65 (1), 133–148, DOI 10.1016/S0168-3659(99)00246-1.

(50). Padilla De Jesus OL; Ihre HR; Gagne L; Frechet JMJ; Szoka FC Polyester Dendritic Systems for Drug Delivery Applications: In Vitro and In Vivo Evaluation. Bioconjug. Chem 2002, 13 (3), 453–461, DOI 10.1021/bc010103m. [PubMed: 12009933]

(51). Fuchs S; Kapp T; Otto H; Schoneberg T; Franke P; Gust R; Schluter AD A Surface-Modified Dendrimer Set for Potential Application as Drug Delivery Vehicles: Synthesis, In Vitro Toxicity, and Intracellular Localization. Chem. - Eur. J 2004, 10 (5), 1167–1192, DOI 10.1002/chem.200305386. [PubMed: 15007808]

(52). Morris CJ; Aljayyoussi G; Mansour O; Griffiths P; Gumbleton M Endocytic Uptake, Transport and Macromolecular Interactions of Anionic PAMAM Dendrimers within Lung Tissue. Pharm. Res 2017, 34 (12), 2517–2531, DOI 10.1007/s11095-017-2190-7. [PubMed: 28616685]

(53). Xiong Z; Wang Y; Zhu J; Li X; He Y; Qu J; Shen M; Xia J; Shi X Dendrimers Meet Zwitterions: Development of a Unique Antifouling Nanoplatform for Enhanced Blood Pool, Lymph Node and Tumor CT Imaging. Nanoscale 2017, 9 (34), 12295–12301, DOI 10.1039/C7NR03940A. [PubMed: 28819657]

(54). Lee H; Baker JR; Larson RG Molecular Dynamics Studies of the Size, Shape, and Internal Structure of 0% and 90% Acetylated Fifth-Generation Polyamidoamine Dendrimers in Water and Methanol. J. Phys. Chem. B 2006, 110 (9), 4014–4019, DOI 10.1021/jp056148s. [PubMed: 16509691]

(55). Maiti PK; Qağin T; Lin S-T; Goddard WA Effect of Solvent and PH on the Structure of PAMAM Dendrimers. Macromolecules 2005, 38 (3), 979–991, DOI 10.1021/ma049168l.

(56). Suek NW; Lamm MH Effect of Terminal Group Modification on the Solution Properties of Dendrimers: A Molecular Dynamics Simulation Study. Macromolecules 2006, 39 (12), 4247–4255, DOI 10.1021/ma060177z.

(57). Lard M; Kim SH; Lin S; Bhattacharya P; Ke PC; Lamm MH Fluorescence Resonance Energy Transfer between Phenanthrene and PAMAM Dendrimers. Phys. Chem. Chem. Phys 2010, 12 (32), 9285–9291, DOI 10.1039/B924522G. [PubMed: 20571614]

(58). Shcharbin D; Janicka M; Wasiak M; Palecz B; Przybyszewska M; Zaborski M; Bryszewska M Serum Albumins Have Five Sites for Binding of Cationic Dendrimers. Biochim. Biophys. Acta BBA - Proteins Proteomics 2007, 1774 (7), 946–951, DOI 10.1016/j.bbapap.2007.04.016. [PubMed: 17560838]

(59). Froehlich E; Mandeville JS; Jennings CJ; Sedaghat-Herati R; Tajmir-Riahi HA Dendrimers Bind Human Serum Albumin. J. Phys. Chem. B 2009, 113 (19), 6986–6993, DOI 10.1021/jp9011119. [PubMed: 19382803]

(60). Ding F; Tsao D; Nie H; Dokholyan NV Ab Initio Folding of Proteins with All-Atom Discrete Molecular Dynamics. Structure 2008, 16 (7), 1010–1018, DOI 10.1016/j.str.2008.03.013. [PubMed: 18611374]

(61). Wang B; Blin T; Kakinen A; Ge X; Pilkington EH; Quinn JF; Whittaker MR; Davis TP; Ke PC; Ding F Brushed Polyethylene Glycol and Phosphorylcholine for Grafting Nanoparticles against Protein Binding. Polym. Chem 2016, 7 (45), 6875–6879, DOI 10.1039/C6PY01480A. [PubMed: 28348639]

(62). Wang B; Seabrook SA; Nedumpully-Govindan P; Chen P; Yin H; Waddington L; Epa VC; Winkler DA; Kirby JK; Ding F; et al. Thermostability and Reversibility of Silver Nanoparticle-Protein Binding. Phys. Chem. Chem. Phys 2014, 17 (3), 17281739, DOI 10.1039/C4CP04996A.

(63). Greene GW; Martin LL; Tabor RF; Michalczyk A; Ackland LM; Horn R Lubricin: A Versatile, Biological Anti-Adhesive with Properties Comparable to Polyethylene Glycol. Biomaterials 2015,53,127–136, DOI 10.1016/j.biomaterials.2015.02.086. [PubMed: 25890713]

(64). Banerjee I; Pangule RC; Kane RS Antifouling Coatings: Recent Developments in the Design of Surfaces That Prevent Fouling by Proteins, Bacteria, and Marine Organisms. Adv. Mater. Deerfield Beach Fla 2011, 23 (6), 690–718, DOI 10.1002/adma.201001215.

(65). Arami H; Khandhar A; Liggitt D; Krishnan KM In Vivo Delivery, Pharmacokinetics, Biodistribution and Toxicity of Iron Oxide Nanoparticles. Chem. Soc. Rev 2015, 44 (23), 8576–8607, DOI 10.1039/C5CS00541H. [PubMed: 26390044]

(66). Garapaty A; Champion JA Non-Covalent Phosphorylcholine Coating Reduces Protein Adsorption and Phagocytic Uptake of Microparticles. Chem. Commun. Camb. Engl 2015, 51 (72), 13814–13817, DOI 10.1039/c5cc03459k.

(67). Cui J; De Rose R; Alt K; Alcantara S; Paterson BM; Liang K; Hu M; Richardson JJ; Yan Y; Jeffery CM; et al. Engineering Poly(Ethylene Glycol) Particles for Improved Biodistribution. ACS Nano 2015, 9 (2), 1571–1580, DOI 10.1021/nn5061578. [PubMed: 25712853]

(68). Blin T; Kakinen A; Pilkington EH; Ivask A; Ding F; Quinn JF; Whittaker MR; Ke PC; Davis TP Synthesis and in Vitro Properties of Iron Oxide Nanoparticles Grafted with Brushed Phosphorylcholine and Polyethylene Glycol. Polym. Chem 2016, 7 (10), 1931–1944, DOI 10.1039/C5PY02024G.

(69). Wang M; Siddiqui G; Gustafsson OJR; Kakinen A; Javed I; Voelcker NH; Creek DJ; Ke PC; Davis TP Plasma Proteome Association and Catalytic Activity of Stealth Polymer-Grafted Iron Oxide Nanoparticles. Small Weinh. Bergstr. Ger 2017, 13 (36), DOI 10.1002/smll.201701528.

(70). Leroueil PR; DiMaggio S; Leistra AN; Blanchette CD; Orme C; Sinniah K; Orr BG; Holl MMB Characterization of Folic Acid and Poly(Amidoamine) Dendrimer Interactions with Folate Binding Protein: A Force-Pulling Study. J. Phys. Chem. B 2015, 119 (35), 11506–11512, DOI 10.1021/acs.jpcb.5b05391. [PubMed: 26256755]

(71). Allen MP; Tildesley DJ Computer Simulation of Liquids; Clarendon Press, 1989.

(72). Rapaport DC The Art of Molecular Dynamics Simulation, 2 edition; Cambridge University Press: Cambridge, UK ; New York, NY, 2004.

(73). Ding F; Dokholyan NV Discrete Molecular Dynamics Simulation of Biomolecules In Computational Modeling of Biological Systems; Dokholyan NV, Ed.; Biological and Medical Physics, Biomedical Engineering; Springer US, 2012; pp 55–73.

(74). Ding F; Dokholyan NV Emergence of Protein Fold Families through Rational Design. PLoS Comput Biol 2006, 2 (7), e85, DOI 10.1371/journal.pcbi.0020085. [PubMed: 16839198]

(75). Yin S; Biedermannova L; Vondrasek J; Dokholyan NV MedusaScore: An Accurate Force Field-Based Scoring Function for Virtual Drug Screening. J. Chem. Inf. Model 2008, 48 (8), 1656–1662, DOI 10.1021/ci8001167. [PubMed: 18672869]

(76). Neria E; Fischer S; Karplus M Simulation of Activation Free Energies in Molecular Systems. J. Chem. Phys 1996, 105, 1902, DOI 10.1063/1.472061.

(77). Lazaridis T; Karplus M Effective Energy Functions for Protein Structure Prediction. Curr. Opin. Struct. Biol 2000, 10 (2), 139–145, DOI 10.1016/S0959-440X(00)00063-4. [PubMed: 10753811]

(78). Ding F; Borreguero JM; Buldyrey SV; Stanley HE; Dokholyan NV Mechanism for the Alpha-Helix to Beta-Hairpin Transition. Proteins 2003, 53 (2), 220–228, DOI 10.1002/prot.10468. [PubMed: 14517973]

(79). Manning GS Limiting Laws and Counterion Condensation in Polyelectrolyte Solutions I. Colligative Properties. J. Chem. Phys 1969, 51 (3), 924–933, DOI 10.1063/1.1672157.

(80). Andersen HC Molecular Dynamics Simulations at Constant Pressure and/or Temperature. J. Chem. Phys 1980, 72 (4), 2384–2393, DOI 10.1063/1.439486.

(81). Shirvanyants D; Ding F; Tsao D; Ramachandran S; Dokholyan NV Discrete Molecular Dynamics: An Efficient And Versatile Simulation Method For Fine Protein Characterization. J. Phys. Chem. B 2012, 116 (29), 8375–8382, DOI 10.1021/jp2114576. [PubMed: 22280505]

(82). Nedumpully-Govindan P; Jemec DB; Ding F CSAR Benchmark of Flexible MedusaDock in Affinity Prediction and Nativelike Binding Pose Selection. J. Chem. Inf. Model 2015, DOI 10.1021/acs.jcim.5b00303.

(83). Berman HM; Westbrook J; Feng Z; Gilliland G; Bhat TN; Weissig H; Shindyalov IN; Bourne PE The Protein Data Bank. Nucleic Acids Res 2000, 28 (1), 235–242. [PubMed: 10592235]

(84). Vuong QV; Nguyen TT; Li MS A New Method for Navigating Optimal Direction for Pulling Ligand from Binding Pocket: Application to Ranking Binding Affinity by Steered Molecular Dynamics. J. Chem. Inf. Model 2015, 55 (12), 2731–2738, DOI 10.1021/acs.jcim.5b00386. [PubMed: 26595261]

(85). Ganesan A; Coote ML; Barakat K Molecular 'Time-Machines' to Unravel Key Biological Events for Drug Design. Wiley Interdiscip. Rev. Comput. Mol. Sci 2017, 7 (4), e1306, DOI 10.1002/wcms.1306.

(86). Isralewitz B; Gao M; Schulten K Steered Molecular Dynamics and Mechanical Functions of Proteins. Curr. Opin. Struct. Biol 2001, 11 (2), 224–230. [PubMed: 11297932]

(87). Kumar S; Li MS Biomolecules under Mechanical Force. Phys. Rep 2010, 486 (1), 1–74, DOI 10.1016/j.physrep.2009.11.001.

(88). Kesner BA; Ding F; Temple BR; Dokholyan NV N-Terminal Strands of Filamin Ig Domains Act as a Conformational Switch under Biological Forces. Proteins 2010, 78 (1), 12–24, DOI 10.1002/prot.22479. [PubMed: 19514078]

(89). Redner S A Guide to First-Passage Processes /core/books/a-guide-to-first-passage- processes/59066FD9754B42D22B028E33726D1F07 (accessed Apr 29, 2018), DOI 10.1017/CBO9780511606014.

(90). Likos CN; Schmidt M; Lowen H; Ballauff M; Potschke D; Lindner P Soft Interaction between Dissolved Flexible Dendrimers: Theory and Experiment. Macromolecules 2001, 34 (9), 2914–2920, DOI 10.1021/ma001346x.

(91). Turro NJ; Lei X-G; Ananthapadmanabhan KP; Aronson M Spectroscopic Probe Analysis of Protein-Surfactant Interactions: The BSA/SDS System. Langmuir 1995, 11, 2525–2533, DOI 10.1021/la00007a035.

(92). Chiba F; Mann G; Twyman LJ Investigating Possible Changes in Protein Structure during Dendrimer-Protein Binding. Org. Biomol. Chem 2010, 8 (22), 5056–5058, DOI 10.1039/C0OB00041H. [PubMed: 20862438]

(93). Anand U; Mukherjee S Binding, Unfolding and Refolding Dynamics of Serum Albumins. Biochim. Biophys. Acta BBA - Gen. Subj 2013, 1830 (12), 5394–5404, DOI 10.1016/j.bbagen.2013.05.017.

(94). Fang M; Cheng Y; Zhang J; Wu Q; Hu J; Zhao L; Xu T New Insights into Interactions between Dendrimers and Surfactants. 4. Fast-Exchange/Slow-Exchange Transitions in the Structure of Dendrimer-Surfactant Aggregates. J. Phys. Chem. B 2010, 114 (18), 6048–6055, DOI 10.1021/jp100805u. [PubMed: 20394447]

(95). Jones PT; Dear PH; Foote J; Neuberger MS; Winter G Replacing the Complementarity-Determining Regions in a Human Antibody with Those from a Mouse. Nature 1986, 321 (6069), 522–525, DOI 10.1038/321522a0. [PubMed: 3713831]

(96). Chlewicki LK; Holler PD; Monti BC; Clutter MR; Kranz DM High-Affinity, Peptide-Specific T Cell Receptors Can Be Generated by Mutations in CDR1, CDR2 or CDR3. J. Mol. Biol 2005, 346 (1), 223–239, DOI 10.1016/j.jmb.2004.11.057. [PubMed: 15663940]

(97). Zhang J-L; Zheng Q-C; Chu W-T; Zhang H-X Drug Design Benefits from Molecular Dynamics: Some Examples. Curr. Comput. Aided Drug Des 2013, 9 (4), 532546.

(98). Kalyaanamoorthy S; Chen Y-PP Modelling and Enhanced Molecular Dynamics to Steer Structure-Based Drug Discovery. Prog. Biophys. Mol. Biol 2014, 114 (3), 123–136, DOI 10.1016/j.pbiomolbio.2013.06.004. [PubMed: 23827463]

(99). Chanphai P; Froehlich E; Mandeville JS; Tajmir-Riahi HA Protein Conjugation with PAMAM Nanoparticles: Microscopic and Thermodynamic Analysis. Colloids Surf. B Biointerfaces 2017, 150, 168–174, DOI 10.1016/j.colsurfb.2016.11.037. [PubMed: 27914253]

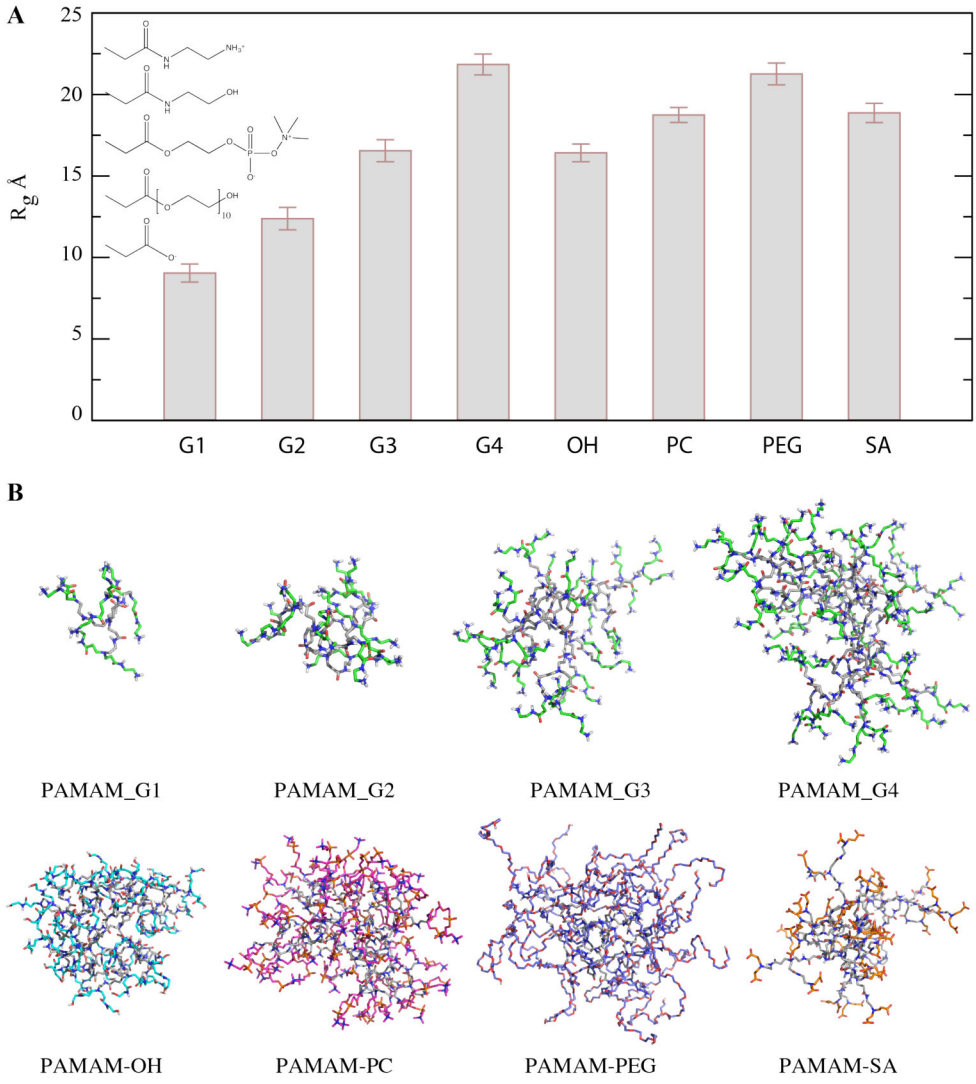

Figure 1. DMD simulations of dendrimers with different sizes and surface modifications.

(A) The averaged Rg of PAMAM dendrimers derived from DMD simulations. Eight PAMAM dendrimers include unmodified PAMAM from G1 to G4, negative charged PAMAM dendrimer (PAMAM-SA), and surface modified by hydroxyl (OH), polyethylene glycol (PEG), and phosphorylcholine (PC). The error bars corresponded to the standard error of mean (SEM) from independent simulations. From top to bottom, the schematic chemical structures for amine, OH, PC, PEG, and SA-terminated groups are given in the inset. (B) Snapshot structures from equilibrated DMD simulations are shown in stick representations for each of the eight types of PAMAM dendrimers. The terminal groups are shown in different colors - amine group in blue, OH in cyan, PC in purple, PEG in wheat, and SA in orange.

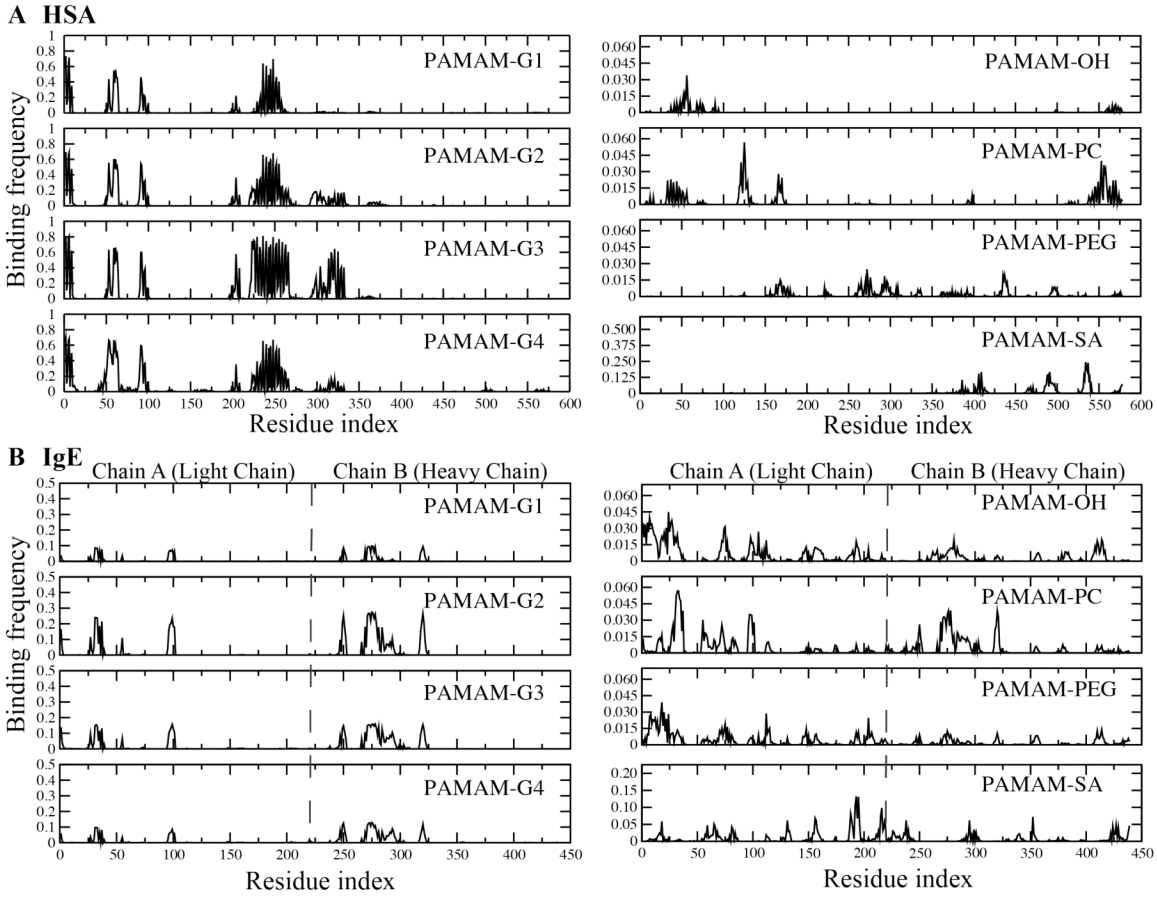

Figure 2. The reside-wise binding frequencies of different proteins with different dendrimers.

(A) The binding of HSA residues with eight different dendrimers. Residues was reindexed to start from 1 instead of 5 as in the PDB. (B) The binding of IgE residues with eight different dendrimers. Residue index form 1 to 219 corresponds to Chain A (the Light Chain) and residues from 220 to 439 form Chain B (the Heavy Chain). The dashed vertical lines are used to indicate the chain separation.

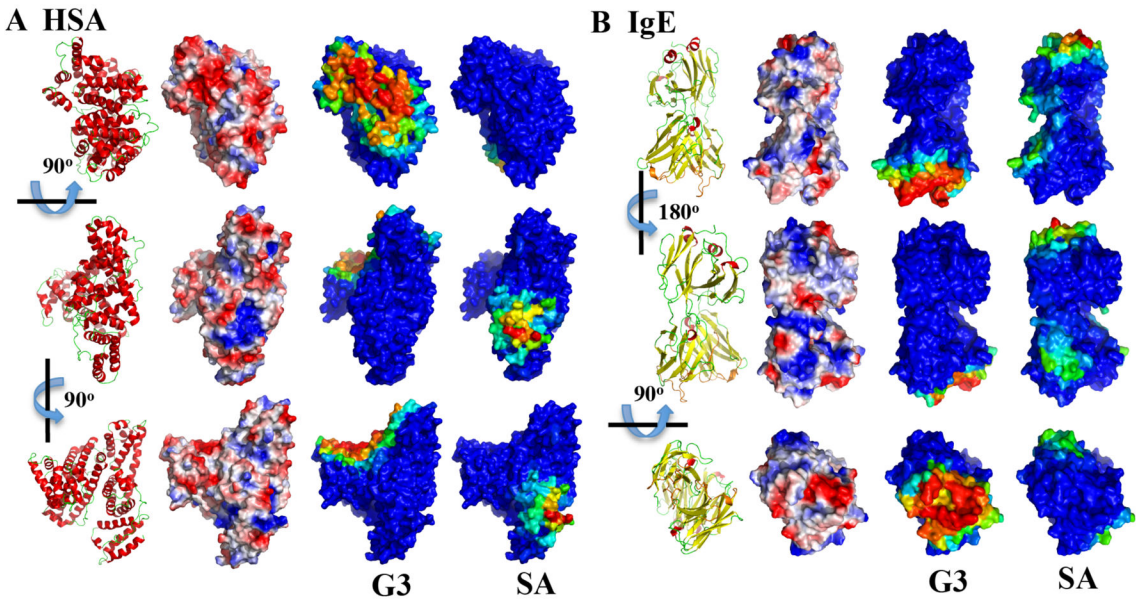

Figure 3. Mapping of protein residues with their binding frequencies to charged dendrimers.

Since all PAMAM G1-G4 had similar per residue binding profile (Fig. 2), only the PAMAM-G3 is shown here. For both (A) HSA and (B) IgE, three different views are shown as indicated by the rotation axes and angles. For comparison, the protein structures in cartoon representation (red for helix, yellow for strand, and green for loop) and the protein surface electrostatic potentials computed by the PyMol (colored from negative potential in red to positive potential in blue) are shown in the first and second column. For the binding with PAMAM-G3 and PAMAM-SA, protein surfaces are colored according to each residue's binding frequency to the dendrimer, in rainbow colors from blue (low) to red (high).

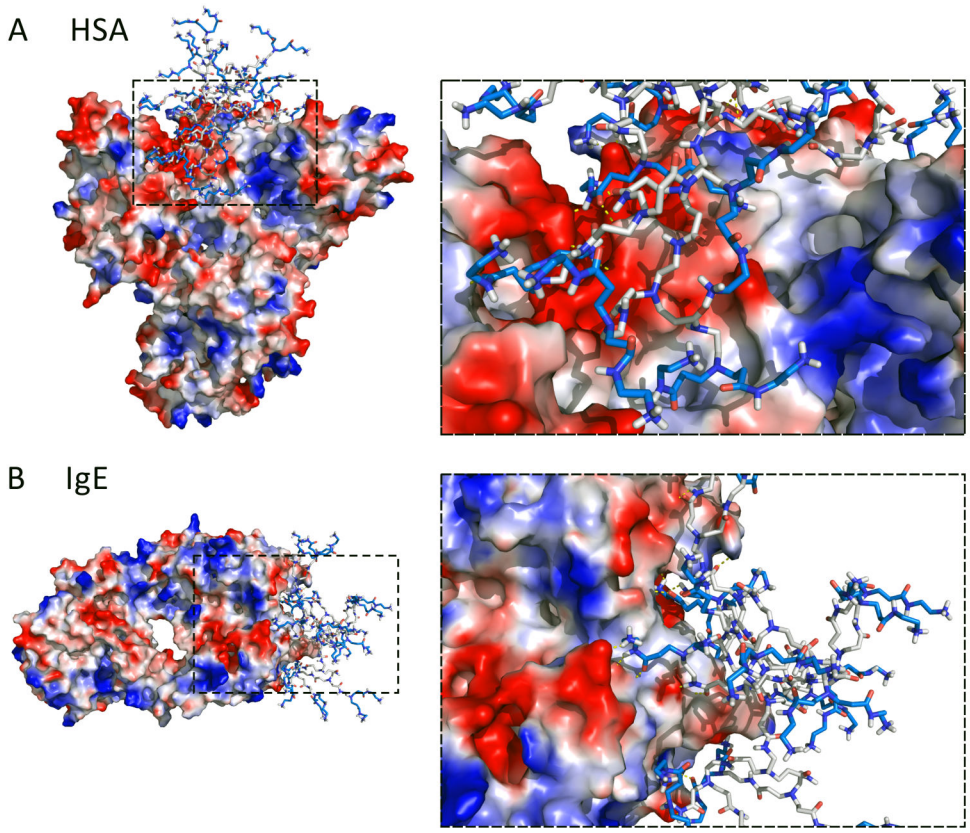

Figure 4. Snapshots of (A) PAMAM-G3-HSA and (B) PAMAM-G3-IgE complexes from DMD simulations.

The protein surfaces are colored from the negative electrostatic potentials in red to the positive potentials in blue. Accordingly, the positively charged surface groups of PAMAM are also colored in blue, while the hydrophobic dendrimer interior is colored in grey. Hydrgen bondsonds between PAMAM and proteins are denoted in yellow dashed-lines in zoom-in snapshots to the right.

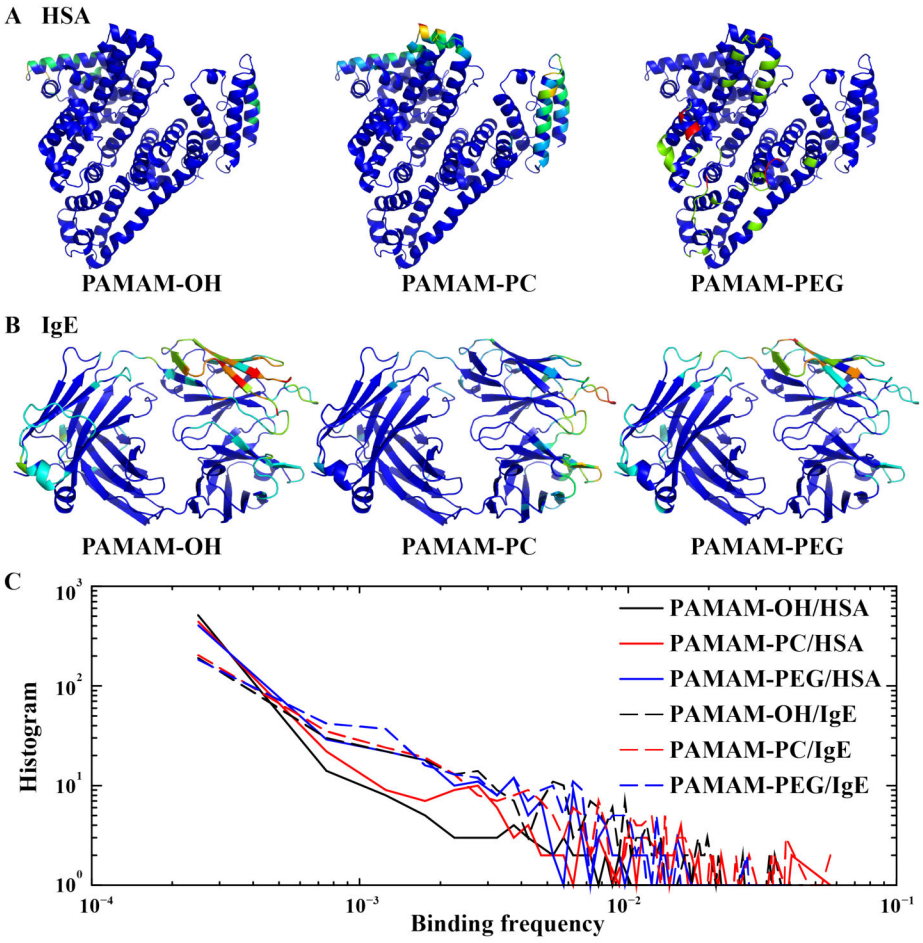

Figure 5. The binding of neutrally charged dendrimers with proteins.

Both (A) HSA and (B) IgE are shown in cartoon representation, and are colored according to each residue's binding frequencies to the dendrimer in rainbow colors from blue (low) to red (high). (C) For each protein-dendrimer pair, the histogram of residue-wise binding frequencies computed from data in Fig. 2 is shown as a log-log plot.

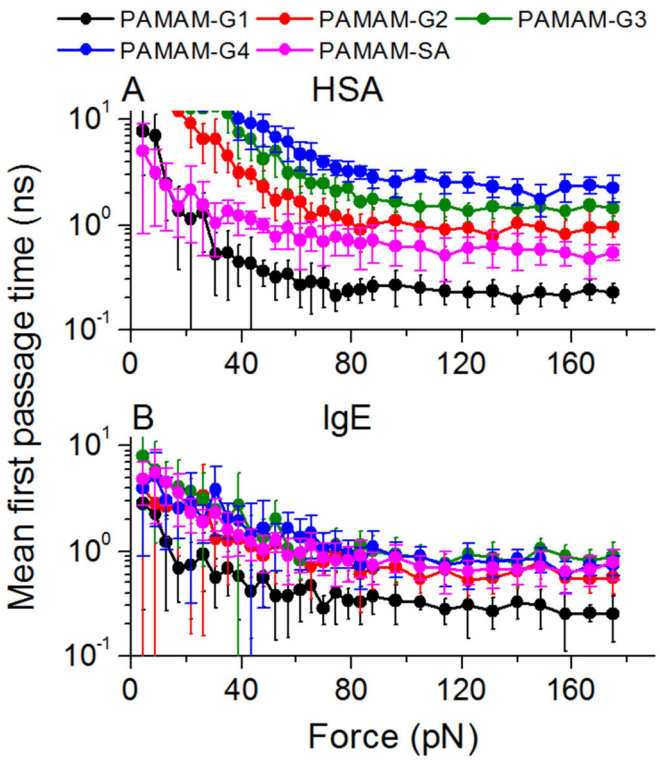

Figure 6. Steered DMD simulations of stable protein-dendrimer complex by charged PAMAM dendrimers.

The mean first passage time for dissociation as a function of pulling forces between dendrimer and (A) HSA or (B) IgE.

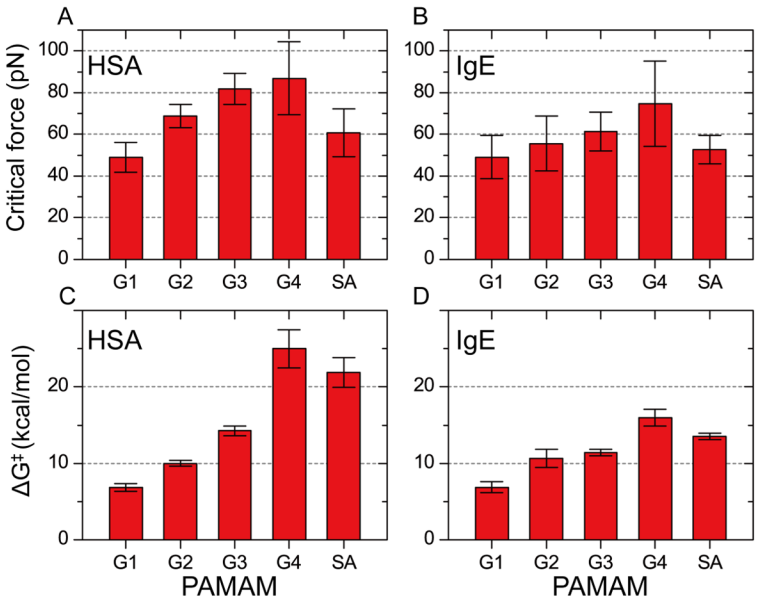

Figure 7. The SDMD analysis of the binding between the protein and dendrimer complex.
The critical forces and the free energy barriers for dissociation estimated for dendrimer binding with (A,C) HSA and with (B,D) IgE.

Table 1.

Binding parameters of dendrimers with HSA.

		PAMAM-G1	PAMAM-G2	PAMAM-G3	PAMAM-G4	-SA	-OH	PEG-G3	PEG-G4
K_b (M^{-1})	*Ref.*[45]	$2.83\pm0.78 \times 10^5$	$2.91\pm0.41 \times 10^5$	$3.65\pm0.75 \times 10^5$	$1.67\pm0.15 \times 10^6$	$2.52\pm0.75 \times 10^6$	$1.29\pm0.93 \times 10^4$		$1.77\pm0.28 \times 10^4$
	Ref.[59]				$2.6\pm0.5 \times 10^4$			$1.3\pm0.2 \times 10^4$	$2.2\pm0.4 \times 10^4$
	Ref.[99]				1.38×10^5				
$\Delta G^{\neq}$ (Kcal/Mol), This work		6.9±1.0	10.0±0.8	14.3±1.3	25.0±5.0	21.9±4.1			